

Subradiance dynamics in a singly-excited chiral-coupled atomic chain

H. H. Jen,^{1,*} M.-S. Chang,² G.-D. Lin,³ and Y.-C. Chen²

¹*Institute of Physics, Academia Sinica, Taipei 11529, Taiwan*

²*Institute of Atomic and Molecular Sciences, Academia Sinica, Taipei 10617, Taiwan*

³*Department of Physics, National Taiwan University, Taipei 10617, Taiwan*
(Dated: May 3, 2019)

We theoretically investigate the subradiance dynamics in a nonreciprocal chiral-coupled atomic chain, in which infinite-range dipole-dipole interaction emerges in the dissipation. We find that super- and subradiance are both present in the dissipation process following single photon excitation, and the decay dynamics shows burst emissions from uniform initial excitations, which reflects the influence of atomic ordering on the propagation of quantum coherence. By tuning the nonreciprocal couplings in the chiral-coupled atomic system, we show that the subradiance dynamics can be greatly modified. We further study the effect of atomic local disorder, and find occurrence of plateaus on the decay curve dependent on the defect locations, as well as persistent localized excitations induced by disorders. Our results show rich opportunities in the chiral-coupled system toward photon storage and routing.

I. INTRODUCTION

Chiral quantum optics [1], a new paradigm of controlling light-matter interactions in one-dimensional (1D) nanophotonics devices [2], opens up many opportunities in quantum information processing and quantum simulation. Chiral coupling allows a nonreciprocal atom-light interface, which breaks the time-reversal symmetry in conventional light-matter interacting systems in free space. This nonreciprocal coupling emerges due to the strong radial confinement of 1D reservoirs which couples the atoms and spontaneously radiates only in the guided dimension [3]. The chiral-coupled interface can be realized in the setting of evanescent waves [4, 5] at the glass-air surface under total internal reflection. Due to considerable reduction of the evanescent waves in the normal direction of the surface, the longitudinal component of light becomes finite and enables the transverse spin angular momentum that can be locked to the propagation direction. This spin-momentum locking or spin-orbital coupling is the essential element in the chiral-coupled systems.

There are important applications in such 1D atom-light interacting systems. In an atom-fiber coupled system, directional spontaneous emissions can be controlled by the internal states of the atoms [6]. In an atom-resonator system, photon routing can be achieved by single-atom switch controlled by the single photon, in which a reflection of the photon toggles the switch from reflection to high transmission [7]. Other than these atom-light interfaces, quantum dot displaced from the crossing region of in-plane nanowire waveguides [8] can guide photons and provide an interface between a solid-state spin qubit and path-encoded photons. Similarly in the setting of quantum dot in the glide-plane photonic crystal waveguide [9] under external magnetic field, chiral coupling of the system realizes a Mach-Zehnder interferometer. Even a CNOT gate can potentially be implemented in such systems [9]. In the setting of two superconducting qubits in a 1D waveguide, nonreciprocal coupling can also be realized via quantum non-

linear couplings under quasi-dark state [10].

Recently, protocols of quantum state transfer using chiral-coupled photonic quantum link were theoretically proposed [11], and selective transport of atomic excitations can be achieved in a driven chiral-coupled atomic chain [12]. Chiral-coupled 1D atomic chain can even realize quantum many-body states of spin dimers [13–15] or simulate exotic photonic topological quantum states [1]. On the recent progress of 1D reciprocally-coupled atom-light systems, protocols were proposed to create mesoscopic entangled states by engineering the collective decay dynamics [3], which revealed emerging universal behavior in the coherent dynamics, i.e., collective frequency shift of the resonant dipole-dipole interaction, of the systems [16].

In this article, we investigate the dynamics of the spontaneous emissions in the 1D chiral-coupled atomic chain as in Fig. 1, since clear identification of super- [17–27] and subradiance [28–38] in such system is less studied. Additionally, since the 1D reservoir allows nonreciprocal decay channels and can be tailored via manipulation of atomic separations and/or excitation beam profiles, the cooperative radiation along the allowed dimension should possess qualitatively different features compared to that in reciprocally-coupled systems.

The rest of the paper is organized as follows. In Sec. II, we obtain the coupling matrix for a 1D chiral-coupled atomic chain with single excitation, and analyze few-atom cases. In Sec. III, we characterize the subradiance for longer atomic chains. In Sec. IV, we further study the effect of dislocations of the atoms on the radiation properties. Finally we conclude in Sec. V. In the Appendix, we review the general formalism for resonant dipole-dipole interaction (RDDI) of the spontaneous emissions in 1D, two-dimensional (2D), and three-dimensional (3D) reservoirs [18].

II. CHIRAL COUPLING MATRIX IN SINGLE EXCITATION HILBERT SPACE

Conventional light-matter interacting systems does not constrain which direction spontaneous emission should radiate

* sappyjen@gmail.com

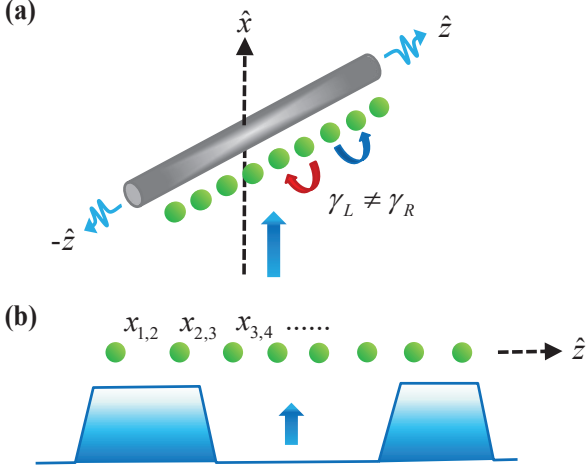


FIG. 1. Chiral-coupled atomic chain. (a) Schematic one-dimensional atom-fiber coupled system demonstrates one example of the chiral coupling. Single photon propagating in \hat{x} excites the atomic chain distributed along \hat{z} near the fiber, and the atom-fiber coupled system guides the spontaneous emissions with the nonreciprocal couplings $\gamma_L \neq \gamma_R$. (b) Illustrative structured beams which non-uniformly excite the atomic chain. Controlled beam profiles and/or inter-atomic separations $x_{1,2}, x_{2,3}, x_{3,4}, \dots$, allow tailoring the state initializations which modify the cooperative couplings.

into; therefore, the RDDI symmetrically couples every pair of atoms in the system, and we should have the reciprocal form of RDDI, which preserves the time reversal symmetry of light scattering, and this property should also preserve in 1D and 2D spaces of reservoirs.

In contrast to the RDDI which we generally obtain and review in the Appendix, the chiral-coupled system allows non-reciprocal decay channels which break the time reversal symmetry. The effective chiral master equation of 1D coupled atom-light interacting system in Lindblad forms [15] gives

$$\frac{dQ}{dt} = -\frac{i}{\hbar}[Q, H_L + H_R] + \mathcal{L}_L[Q] + \mathcal{L}_R[Q], \quad (1)$$

where

$$H_L \equiv -\frac{i\hbar\gamma_L}{2} \sum_{\mu < \nu} \left(e^{ik|x_\mu - x_\nu|} \sigma_\mu^\dagger \sigma_\nu - \text{H.c.} \right), \quad (2)$$

$$H_R \equiv -\frac{i\hbar\gamma_R}{2} \sum_{\mu > \nu} \left(e^{ik|x_\mu - x_\nu|} \sigma_\mu^\dagger \sigma_\nu - \text{H.c.} \right), \quad (3)$$

denote the RDDI energy shifts, and the Lindblad forms,

$$\mathcal{L}_L[\hat{Q}] \equiv -\frac{\gamma_L}{2} \sum_{\mu, \nu} \left\{ e^{-ik(x_\mu - x_\nu)} (\sigma_\mu^\dagger \sigma_\nu Q + Q \sigma_\mu^\dagger \sigma_\nu - 2\sigma_\mu^\dagger Q \sigma_\nu) \right\}, \quad (4)$$

$$\mathcal{L}_R[\hat{Q}] \equiv -\frac{\gamma_R}{2} \sum_{\mu, \nu} \left\{ e^{ik(x_\mu - x_\nu)} (\sigma_\mu^\dagger \sigma_\nu Q + Q \sigma_\mu^\dagger \sigma_\nu - 2\sigma_\mu^\dagger Q \sigma_\nu) \right\}, \quad (5)$$

characterize the cooperative spontaneous decay under RDDI. The subscripts L and R respectively indicate the left- and right-propagating components of the 1D RDDI. We first note that the Lindblad forms here do not include non-guided couplings or other non-radiative losses, which could present in fibers or waveguides and reduce the overall efficiency of light collection. Furthermore, for atoms confined in 1D, we have ordering on the atomic positions, $x_1 < x_2 < \dots < x_{N-1} < x_N$, which otherwise does not present in the 2D and 3D cases, and we show in the below that this atomic ordering plays a role on cooperative spontaneous emissions.

When $\gamma_L = \gamma_R = \gamma$, we retrieve the usual reciprocal and infinite-range couplings of Eq. (A.12),

$$J_{\mu, \nu} = \frac{\Gamma_{1D}}{2} [\cos(k_L x_{\mu, \nu}) + i \sin(k_L |x_{\mu, \nu}|)], \quad (6)$$

where $\Gamma_{1D} = 2\gamma$ and $J_{\mu, \nu} = J_{\nu, \mu}$. $\text{Re}[J_{\mu, \nu}]$ and $\text{Im}[J_{\mu, \nu}]$ denote the incoherent and coherent parts of the couplings respectively. This infinite-range and cooperative dipole-dipole interaction in the 1D atom-fiber coupled system has been investigated theoretically [39–41] and recently observed in macroscopically separated cold atoms [42].

When single photon interacts with the atomic chain, only one of the atoms is excited. By defining

$$F_{\mu\nu} \equiv \frac{\gamma_R e^{ik|x_{\mu,\nu}|} + \gamma_L e^{-ik|x_{\mu,\nu}|}}{2}, \quad (7)$$

$$G_{\mu\nu} \equiv -i \frac{\gamma_R e^{ik|x_{\mu,\nu}|} - \gamma_L e^{-ik|x_{\mu,\nu}|}}{2}, \quad (8)$$

and in terms of single excitation space $|\psi_\mu\rangle = |e\rangle_\mu |g\rangle^{\otimes(N-1)}$, we obtain the interaction Hamiltonian,

$$V = \begin{bmatrix} -F_{11} & -F_{12} + iG_{12} & -F_{13} + iG_{13} & \dots & -F_{1N} + iG_{1N} \\ -F_{12}^* + iG_{12}^* & -F_{22} & -F_{23} + iG_{23} & \dots & -F_{2N} + iG_{2N} \\ -F_{13}^* + iG_{13}^* & -F_{23}^* + iG_{23}^* & -F_{33} & \dots & -F_{3N} + iG_{3N} \\ \vdots & \vdots & \vdots & \ddots & \vdots \\ -F_{1N}^* + iG_{1N}^* & -F_{2N}^* + iG_{2N}^* & -F_{3N}^* + iG_{3N}^* & \dots & -F_{NN} \end{bmatrix}. \quad (9)$$

The atomic dynamics $|\Psi(t)\rangle = \sum_\mu c_\mu(t) |\psi_\mu\rangle$ is determined by the coupled equations: $\dot{c}_\mu = \sum_\nu V_{\mu, \nu} c_\nu$. In general, $F_{\mu\nu}$ and $G_{\mu\nu}$ are complex numbers, and V is reciprocal, viz $V_{\mu, \nu} = V_{\nu, \mu}$, under $\gamma_L = \gamma_R = \gamma$.

By expressing V as

$$V = \begin{bmatrix} -\frac{\gamma_L + \gamma_R}{2} & -\gamma_L e^{-ik|x_{1,2}|} & -\gamma_L e^{-ik|x_{1,3}|} & \dots & -\gamma_L e^{-ik|x_{1,N}|} \\ -\gamma_R e^{-ik|x_{1,2}|} & -\frac{\gamma_L + \gamma_R}{2} & -\gamma_L e^{-ik|x_{2,3}|} & \dots & -\gamma_L e^{-ik|x_{2,N}|} \\ -\gamma_R e^{-ik|x_{1,3}|} & -\gamma_R e^{-ik|x_{2,3}|} & -\frac{\gamma_L + \gamma_R}{2} & \dots & -\gamma_L e^{-ik|x_{3,N}|} \\ \vdots & \vdots & \vdots & \ddots & \vdots \\ -\gamma_R e^{-ik|x_{1,N}|} & -\gamma_R e^{-ik|x_{2,N}|} & -\gamma_R e^{-ik|x_{3,N}|} & \dots & -\frac{\gamma_L + \gamma_R}{2} \end{bmatrix}, \quad (10)$$

the nonsymmetric feature of chiral coupling matrix emerges when $\gamma_R \neq \gamma_L$, and V becomes nonreciprocal as $VV^\dagger \neq V^\dagger V$. The system dynamics can be solved directly from

$$\frac{d}{dt}\vec{c} = V\vec{c}, \quad (11)$$

where $\vec{c} \equiv [c_1(t), c_2(t), \dots, c_N(t)]$ with given initial conditions of $\vec{c}(t=0)$. Below we show analytical results for few-atom systems, and throughout the paper we consider uniform excitations of the atomic chain.

A. Cascaded scheme

First we investigate two and three atoms in the cascaded scheme [13, 43, 44] where one of the nonreciprocal couplings $\gamma_{L,R}$ is zero, so that only unidirectional coupling is permitted. Starting with two atoms, we have the coupled equations,

$$\dot{c}_1(t) = -\frac{\gamma_L + \gamma_R}{2}c_1(t) - \gamma_L e^{-i\xi}c_2(t), \quad (12)$$

$$\dot{c}_2(t) = -\gamma_R e^{-i\xi}c_1(t) - \frac{\gamma_L + \gamma_R}{2}c_2(t), \quad (13)$$

where $\xi \equiv k|x_{1,2}|$, and correspondingly $\xi\lambda/(2\pi)$ represents the atomic separation $|x_{1,2}|$, given the transition wavelength λ . For reciprocal couplings where $\gamma_L = \gamma_R$ and assume $\xi = 0$ or 2π , we retrieve the conventional results of Dicke's super- and subradiance when $c_1(0) = 1/\sqrt{2}$ and $c_2(0) = \pm 1/\sqrt{2}$, respectively. They give the symmetric and anti-symmetric states of single excitation spaces, $(|ge\rangle \pm |eg\rangle)/\sqrt{2}$. For an arbitrary ξ , with uniform excitations $c_1(0) = 1/\sqrt{2}$, $c_2(0) = 1/\sqrt{2}$, and considering the extreme case of nonreciprocal couplings in the cascaded scheme [13] where $\gamma_L = 0$ and $\gamma_R = \gamma$, we can solve for the above coupled equations,

$$c_1(t) = \frac{1}{\sqrt{2}}e^{-\gamma t/2}, \quad (14)$$

$$c_2(t) = \frac{1}{\sqrt{2}}e^{-\gamma t/2}(1 - \gamma t e^{-i\xi}). \quad (15)$$

For three atoms, we have the coupled equations,

$$\dot{c}_1(t) = -\frac{\gamma_L + \gamma_R}{2}c_1(t) - \gamma_L e^{-i\xi}c_2(t) - \gamma_L e^{-i2\xi}c_3(t), \quad (16)$$

$$\dot{c}_2(t) = -\gamma_R e^{-i\xi}c_1(t) - \frac{\gamma_L + \gamma_R}{2}c_2(t) - \gamma_L e^{-i\xi}c_3(t), \quad (17)$$

$$\dot{c}_3(t) = -\gamma_R e^{-i2\xi}c_1(t) - \gamma_R e^{-i\xi}c_2(t) - \frac{\gamma_L + \gamma_R}{2}c_3(t), \quad (18)$$

where uniform distributions of an atomic array is reflected on the phases $e^{-im\xi}$ with integers m . For the extreme case of $\gamma_L = 0$, $\gamma_R = \gamma$, with the initial condition of uniform excitations $c_{1,2,3}(0) = 1/\sqrt{3}$, we obtain

$$c_1(t) = \frac{e^{-\gamma t/2}}{\sqrt{3}}, \quad (19)$$

$$c_2(t) = \frac{e^{-\gamma t/2}(1 - \gamma t e^{-i\xi})}{\sqrt{3}}, \quad (20)$$

$$c_3(t) = \frac{e^{-\gamma t/2}[\gamma^2 t^2 e^{-i2\xi} - 2\gamma t(e^{-i\xi} + e^{-i2\xi}) + 2]}{2\sqrt{3}}. \quad (21)$$

In Fig. 2, we plot the excited state populations at specific ξ in the cascaded scheme when $\gamma_R = 0$, for two- and three-atom cases. As shown in Eqs. (14) and (19), the excited state population of the leftmost atom always decays as in the single atom (noninteracting) regime, which has a time dependence of $e^{-\gamma t}$, since there is no coupling to this atom from the atoms on the right. We find that at $\xi \lesssim \pi/4$, the total population $P_{tot}(t) = \sum_m P_m(t) \equiv |c_m(t)|^2$ shows an early superradiant decay followed by a subradiance, which can be seen in the upper panels of Fig. 2(a) and 2(b). The subradiant decay originates from the re-excitation of the atoms on the right by the (virtual) photon coming from the left, and this is deterministically achieved due to the quantum coherences between the atoms. For even larger ξ up to π , $P_{tot}(t)$ always decays subradiantly, and the repopulation emerges at different times depending on ξ . Specifically in the lowest plot of Fig. 2(b) for $\xi = \pi$, the atoms orderly repopulate the excited state and decay, i.e. $P_3(t)$ decays after $P_2(t)$. This indicates that the light excitation from the left can only transfer to the atoms on the right, blocking re-excitation of atoms on the left. This is also distinct for a 1D reservoir where light scattering and excitation exchange are allowed in one dimension only. When $\xi \approx \pi$, $P_{tot}(t)$ presents the most subradiant emission, which is reminiscent of the decoherence-free state in the setting with reciprocal couplings.

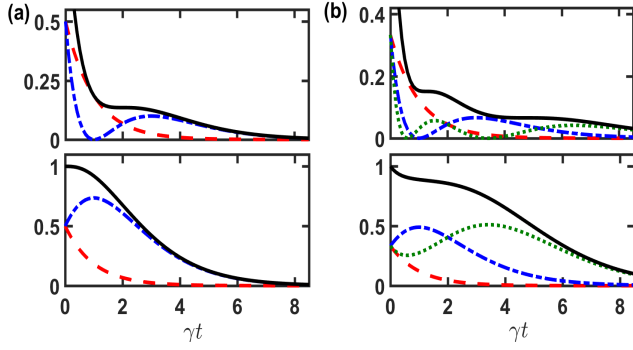


FIG. 2. Excited state populations of few atom systems for $\gamma_R = \gamma$ and $\gamma_L = 0$. (a) For $N = 2$, the upper and lower plots show the cases of $\xi = 0$ and π respectively. The excited state population of the first atom $P_1(t)$ (dashes in red) always decays as single atom $\propto e^{-\gamma t}$, while the second one $P_2(t)$ (dash-dots in blue) decays with repopulation and oscillation in either super- (upper plot) or subradiant rates (lower plot) in a short term. The total excited state population (solid line in black) shows nontrivial decay behaviors. (b) Excited state populations for $N = 3$ with corresponding ξ 's in (a). In long time limit, the third atom (dots in green) decays slower than the second one (dash-dots in blue), while the second atom decays slower than the first one (dashes in red).

In such cascaded scheme ($\gamma_L = 0$), only unidirectional coupling is allowed, and the re-excitation of the atoms on the right can be seen as the atoms in the setting of 1D reciprocal couplings with a perfect mirror on the left, which reflects the light leaving to the left back to the atoms. This is not possible for a conventional atomic chain without a waveguide, which scatters light in 3D free space. In the next subsection, we further investigate the non-cascaded scheme when γ_L is finite.

B. Non-cascaded scheme

The non-cascaded scheme contrasts with the cascaded one when both left/right couplings are finite. For $N = 2$ and 3, we show $P_{tot}(t)$ in Fig. 3 at two specific $\xi = 0$ and π , which respectively show early superradiant and subradiant behaviors as in the cascaded scheme ($\gamma_L = 0$). At $\xi = 0$ in Fig. 3(a), both $P_{tot}(t)$ decay more superradiantly initially as γ_L increases, which respectively approach $e^{-4\gamma t}$ and $e^{-6\gamma t}$ when $\gamma_L \rightarrow \gamma_R$, significantly faster than $e^{-2\gamma t}$ and $e^{-3\gamma t}$ in the noninteracting regime. This enhancement of superradiance is expected for uniform excitations and finite γ_L at small ξ or $\xi \sim 2\pi$, where all the atoms are in phase as in Dicke's superradiant regime. At much later time, these subradiant tails dissipate faster for smaller γ_L , which indicates of occupations, though fairly small, with longer decay time scales for γ_L close to γ_R .

In Fig. 3(b), we further show the subradiance dynamics at $\xi = \pi$ from cascade, to non-cascade, then to symmetric couplings. For both cases of $N = 2$ and 3, all atomic excitations prolong in time as γ_L increases. This drives the system more subradiant toward decoherence-free states for even N , where $\gamma_L = \gamma_R$ and $P_m(\infty) = N^{-1}$. While for odd N when

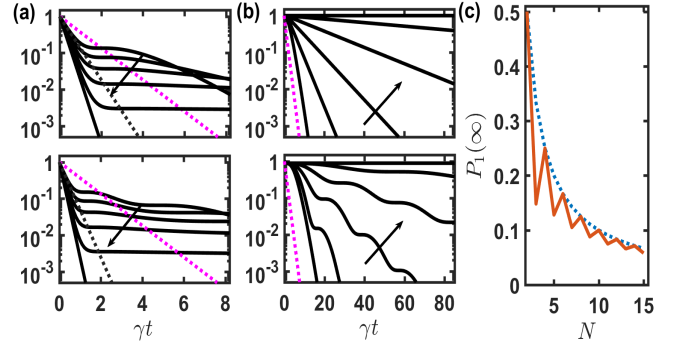


FIG. 3. Excited state populations in the cascaded and non-cascaded scheme. In (a) $\xi = 0$ and (b) $\xi = \pi$, we plot $P_{tot}(t)$ for $N = 2$ and 3 in the upper and lower plots respectively. With a constant $\gamma_R = \gamma$, the arrows indicate the increasing $\gamma_L/\gamma = 0, 0.2, 0.4, 0.6, 0.8$ to 1.0. The dots in magenta give $e^{-\gamma t}$ and is plotted in (a) and (b) as references. The dots in black give $e^{-2\gamma t}$ and $e^{-3\gamma t}$ respectively in the upper and lower plots of (a) as comparisons with noninteracting regime. In (c) when $\gamma_L = \gamma_R$ at $\xi = \pi$, we show $P_1(t \rightarrow \infty)$ (solid), which approaches N^{-1} (dotted) for odd N asymptotically as N increases.

$\gamma_L = \gamma_R$, the system becomes decoherence-free only when $N \rightarrow \infty$ with $P_m(\infty) \rightarrow N^{-1}$. This can be seen in Fig. 3(c) where we show $P_1(\infty)$ as an example. The total excited populations for odd N never reaches one for finite N , and the remaining population should be in the ground state. This reflects that initially uniform excitation can never be decomposed in terms of decoherence-free eigenstates unless $N \rightarrow \infty$. As an example of $N = 3$, the decoherence-free eigenstates are $\vec{c} = [-1, 0, 1]$ and $[1, 1, 0]$, whereas the third eigenstate is $[1, -1, 1]$ with an eigenvalue of -3γ .

In general for odd N at $\xi = \pi$, the atoms on the edges decay faster, which can be seen in Eqs. (16) and (18) in the example of $N = 3$, while they are repumped by the radiation of the central one. As time evolves, the central atom are excited and then decays, transferring the excitation more to the right than to the left given $\gamma_R > \gamma_L$. This leads to atomic population oscillations due to interferences of light transmissions and reflections. These exchanges of excitations play important roles in determining the radiation evolutions in the 1D chiral-coupled system, and manifest different decay behaviors for even and odd N , which we will discuss in the next section. Below we study longer atomic chain with nonreciprocal couplings and investigate the system especially for subradiant dynamics in longer time scales. As a final remark in this section, we note that Dicke's super- and subradiance under reciprocal couplings actually set the maximal and minimal bound of decay constants respectively. Therefore, the nonreciprocal couplings basically destroy (or partially destroy) the coherences required for Dicke's super- and sub-radiance. In other words, the super- and sub-radiant decay behaviors become less significant when the time-reversal symmetry in the couplings is broken.

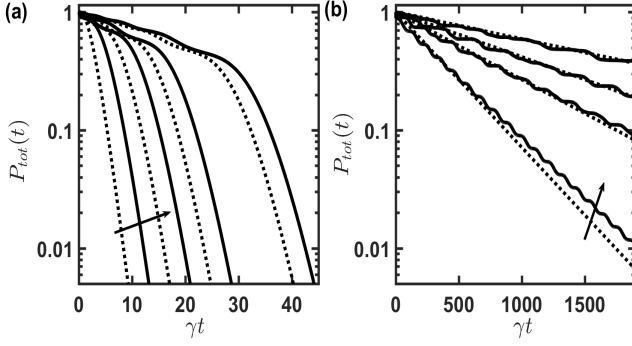


FIG. 4. Subradiance dynamics at $\xi = \pi$. The total atomic populations for (a) the cascaded case of $\gamma_L = 0$ and (b) the non-cascaded case of $\gamma_L = 0.9\gamma_R$ in logarithmic scales. The arrows indicate the increasing N from 2–7 to 10, 11 where we denote the even/odd N as dashed and solid lines respectively. The P_{tot} shows clear plateaued regions of excitations for odd N in (b).

III. SUBRADIANCE FROM A CHIRAL-COUPLED ATOMIC CHAIN

For a longer chiral-coupled atomic chain, we expect many-atom collective behaviors in the decay dynamics. In Fig. 4, we demonstrate the subradiance dynamics at $\xi = \pi$ as we increase N . In the cascaded scheme, the subradiant decay becomes more subradiant as N increases. At least two decay time scales can be seen for the early and later stages of the exponential decay, which is evident in logarithmic plots, in contrast to the conventional exponential decay of noninteracting atoms. As γ_L increases, we expect subradiance at a longer time as indicated in Fig. 3. As an example, we choose γ_L close to γ_R in Fig. 4(b), which presents a clear difference of subradiance between even and odd N . For odd N in general, $P_{tot}(t)$ possesses excitation plateaus. This is due to temporally ordered atomic excitations as the system dissipates. The effect of smaller γ_L modifies the overall decay, which has a shortened lifetime but still maintains the plateaued regions. In contrast to the subradiance of odd N , $P_{tot}(t)$ of even N decays exponentially. This is due to the balanced excitation transfer between the atoms on even and odd sites. The ordered individual excitations from an odd N atomic chain originates from the imbalanced population transfer, which can be seen in the early stage of the cases of $\xi = \pi$ in Figs. 2. The quantum correlations between any two atoms in an odd N atomic chain are further modified by the unpaired particle, which results in a π phase change of the coherences $C_{nn'}(t) = c_n(t)c_{n'}^*(t)$, in contrast to the case of even N . Therefore, the plateaued excitations reflect this distinctive correlation in odd number of particles in the chiral-coupled chain, and can maintain in the subradiance dynamics.

To compare with experimental observations, in Fig. 5 we numerically calculate the radiation intensity,

$$I_{tot}(t) = -\frac{dP_{tot}(t)}{dt}.$$

The burst emissions can be seen in Fig. 5, which reflects the clear plateaued regions of excitations in Fig. 4. For even N ,

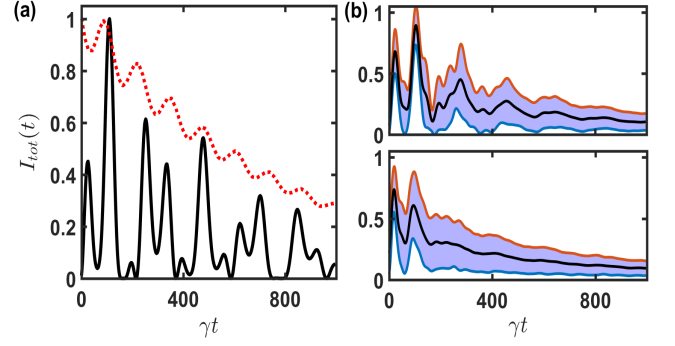


FIG. 5. Radiation dynamics at $\xi = \pi$ in the non-cascaded scheme of $\gamma_L = 0.9\gamma_R$. (a) We show the time evolutions of emissions for the cases of $N = 4$ (dashes in red) and 5 (solid line in black) from the results of Fig. 4. (b) For $N = 5$, we introduce position fluctuations in the upper and lower plots respectively with 0.5% and 1% randomly distributed deviations around the fixed positions. The shaded areas represent 1σ standard deviation of the mean curve (solid line in black) over ensemble averages.

the radiation evolution simply follows the exponential curve with small oscillations, in contrast to the bursts of radiation for odd N . The occurrences of the burst emission can, however, be reduced by position fluctuations. In Fig. 5(b), as the degree of fluctuation increases, the feature of burst radiation disappears. Since the chiral-coupled interactions are sensitively affected by the fluctuations of atomic positions, we expect that our predictions can be observable when the system experiences $< 0.5\%$ of position fluctuations.

IV. EFFECT OF ATOM DISLOCATION

In the above, we discussed subradiance dynamics in ideal conditions. Here we shall discuss non-ideal cases where dislocation of constituent atoms is present. This is necessary, because a precise positioning of the atoms is not easily fulfilled experimentally on the one hand, and on the other hand, disorder is known to induce Anderson localization. It is necessarily of interest to investigate the interplay between cooperative radiation and dislocation. Here the spatial variations of the atoms should be normalized to the transition wavelength. As such the effects of dislocation of superconducting qubits are less significant due to the long transmission wavelength, but for atoms with optical transitions, the effects are much more prominent.

In Fig. 6, we show two examples of destruction and creation of plateaued excitations, where we add a spatial disorder at the level of a fraction of ξ . For odd number of atoms in Fig. 6(a), the central or edge disorder destroys the successive excitations that lead to the plateaued pattern when spatial variation $\gtrsim 3\%$. However, this can be restored when we place the disorder on the even sites for arbitrary spatial variations. This disorder can lead to initial fast decay either itself in Fig. 6(a) or with its neighboring atom in Fig. 6(b), which are negligibly small ($P_m(t) \lesssim 0.01$). For the spatial variation $\lesssim 2\%$, $P_{tot}(t)$ behaves as if no presence of the spatial

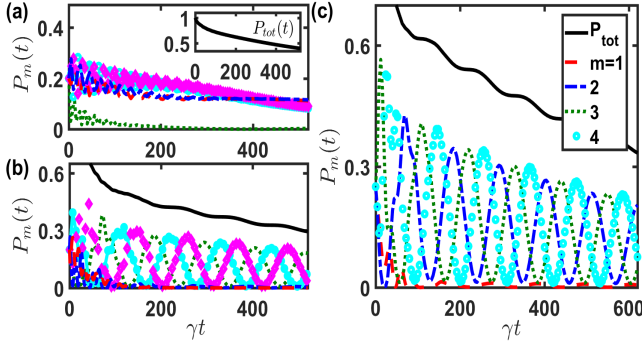


FIG. 6. Disorder-induced plateaued excitations. In the non-cascaded scheme as in Fig. 4 with $N = 5$, $\gamma_L = 0.9\gamma_R$, and $\xi = \pi$, we place the spatial variation of 5% to the right on (a) the central (the third) and (b) the second atoms. No plateaued excitation presents in (a), while plateaus reappear in (b). (c) Similarly for $N = 4$, the leftmost atomic position is varied by 5%, and the plateaued excitation emerges, in contrast to Fig. 4. The respective line symbols for $P_m(t)$ are shown in the legend of (c), and \diamond in magenta is for $m = 5$.

deviation, and beyond which the disorder starts to make an effect on the radiation dynamics. On the other hand for even N in Fig. 6(c), the plateaued excitation emerges due to the edge disorder $\gtrsim 2\%$, in contrast to Fig. 4 where an atomic chain of even number decays exponentially without flattened regions. Clear plateaued regions can be seen and this indicates of spatially-dependent disorder-induced excitation plateaus in a chiral-coupled atomic chain, which allows a controllable way to manipulate the subradiant emission dynamics.

Interestingly, in Fig. 7, when we choose $\xi \sim 3\pi/4$ and introduce a $\sim 30\%$ of position disorder on the n th non-edge atom, $P_n(t)$ and $P_{n-1}(t)$ preserve for a much longer time. This shows disorder-induced localized excitations, which can maintain up to $\gamma t \sim 10^4$ with only around 20% reduction of the $P_{tot}(\gamma t \sim 100)$. Other parameter regimes, for example of $\xi = 2.5\pi/4$ and $\sim 60\%$ disorder, can also support this localized excitation. This demonstrates a dimer-like excitation,

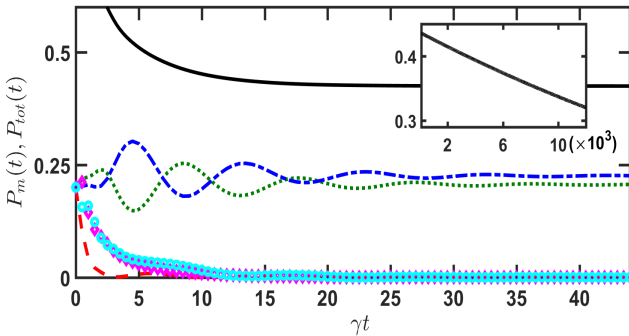


FIG. 7. Disorder-induced persistent localized excitations. In the non-cascaded scheme as in Fig. 4 with $N = 5$, $\gamma_L = 0.9\gamma_R$, but here with $\xi = 3\pi/4$ and 30% spatial variation on the central atom, $P_{2,3}(t)$ sustains at finite populations for a very long time as shown in the inset. The line symbols are the same as in Fig. 6.

which effectively forms a many-body state,

$$\left(\sqrt{1 - P_{n-1} - P_n} + \sqrt{P_{n-1}\sigma_{n-1}^\dagger} + \sqrt{P_n\sigma_n^\dagger} \right) |g\rangle^{\otimes N},$$

which can be prepared for very long time and controlled by local disorders. Moreover, for $n = 2$ or N , $P_{n(n-1)}(t)$ decays much slower than the other $P_{m \neq n}(t)$, but not as the cases of $3 \leq n \leq N - 1$ which extend to a long time. This indicates the edge effect which involves the atoms at the boundary, where they decay to the left or right without back radiations. Nonetheless, the observation of these long-term behaviors can eventually be limited by the losses from non-guided modes.

V. CONCLUSION

In conclusion, we have investigated the subradiant excitations from a chiral-coupled 1D atomic chain, which allows an infinite-range dipole-dipole interaction and nonreciprocal radiation coupling. The subradiance arisen from this non-conventional coupling shows rich dynamics. In this chiral-coupled 1D system where the right and left decay channels are finite but different, we can initiate superradiance or subradiance depending on the inter-atomic spacing in a uniformly distributed atomic chain. When the number of the atoms increases, the subradiant decay rate decreases, which indicates multi-atom enhancement. This non-cascaded scheme also allows sequential radiations from the ordered atoms, which form a series of excitation plateaus due to the violation of the time reversal symmetry, in contrast to the case of reciprocal couplings where m th and $(N - m + 1)$ th atoms should behave exactly the same in time. However, this feature of burst emissions following plateaued excitations is deteriorated by fluctuations of atomic positions, but can be sustained and observable as long as the fluctuations are kept small.

Furthermore, by introducing local disorder in space and strength, the excitation plateaus can be tuned to appear or disappear. We also obtain the disorder-induced localized excitations which can maintain for a very long time. This suggests dynamical dimer-like state components spontaneously emerged from the system via dissipation. An even richer dynamics can be possible for multiple disorders or multi-photon excitations, such that potentially trimerized or complex correlations can emerge in the chiral-coupled system. Finally, our investigations on subradiance is of interest to quantum storage of guided emissions [45], and we also expect potential applications in many-body spin dynamics [46] with chiral and infinite-range couplings.

ACKNOWLEDGEMENTS

This work is supported by the Ministry of Science and Technology (MOST), Taiwan, under the Grant No. MOST-106-2112-M-001-005-MY3, 106-2811-M-001-130, and 107-2811-M-001-1524. GDL thanks the support from MOST of Taiwan under Grant No. 105-2112-M-002-015-MY3 and National Taiwan University under Grant No. NTU-106R891708.

We are also grateful for the support of NCTS ECP1 (Experimental Collaboration Program).

Appendix: Cooperative spontaneous emissions in one- and two-dimensional reservoirs

1. General formalism

Cooperative spontaneous emissions in a three-dimensional (free space) reservoir has been investigated [18], where resonant dipole-dipole interaction (RDDI) in the dissipation process emerges due to the common light fields mediating the whole atomic system. This pairwise dipole-dipole interaction underlies the super- and subradiance which hugely depend on the atomic spatial configurations. These contrasted fast and slow decay phenomena, especially from a dense medium, are originated from nonclassical many-body states [31] accessible in a light-matter interacting system.

Following the line of deriving RDDI in a three-dimensional (3D) reservoir [18], here we review the cooperative spontaneous emissions in one- [3] (1D) and two-dimensional (2D) reservoirs. From a system of N two-level atoms ($|g\rangle$ and $|e\rangle$ for the ground and excited states respectively) interacting with a reservoir composed of quantized bosonic fields, we have the Hamiltonian with a dipole approximation,

$$H = \sum_{\mu=1}^N \hbar\omega_e \hat{\sigma}_{\mu}^{\dagger} \hat{\sigma}_{\mu} - \sum_{\mu=1}^N \sum_q g_q (e^{i\mathbf{k}_q \cdot \mathbf{r}_{\mu} - i\omega_q t} \hat{a}_q + e^{-i\mathbf{k}_q \cdot \mathbf{r}_{\mu} + i\omega_q t} \hat{a}_q^{\dagger}) (\hat{\sigma}_{\mu} + \hat{\sigma}_{\mu}^{\dagger}), \quad (\text{A.1})$$

where $\hat{\sigma}_{\mu} \equiv |g\rangle_{\mu} \langle e|$, and bosonic fields \hat{a}_q should satisfy commutation relations $[\hat{a}_q, \hat{a}_{q'}^{\dagger}] = \delta_{q,q'}$. Note that the above light-matter interaction involves non-rotating wave terms. These often neglected terms (called rotating-wave approximation which is valid since twice the optical frequency of the interacting light field is averaged out) are crucial for a complete

description of the frequency shift (dispersion) in the dissipation, which therefore should satisfy the Kramers-Kronig relation with the decay rate (absorption). The coupling constant is $g_q \equiv d/\hbar\sqrt{\hbar\omega_q/(2\epsilon_0 V)}(\vec{\epsilon}_q \cdot \hat{d})$ with a dipole moment d , unit direction of the dipole \hat{d} , field polarization $\vec{\epsilon}_q$, and quantization volume V .

Consider a Heisenberg equation for an atomic operator \hat{Q} , we have $d\hat{Q}/dt = i[H, \hat{Q}]$ (setting $\hbar = 1$), which reads

$$\frac{d\hat{Q}}{dt} = i\omega_e \sum_{\mu} [\hat{\sigma}_{\mu}^{\dagger} \hat{\sigma}_{\mu}, \hat{Q}] - i \sum_{\mu} \sum_q g_q \{ e^{i\mathbf{k}_q \cdot \mathbf{r}_{\mu}} [\hat{\sigma}_{\mu} + \hat{\sigma}_{\mu}^{\dagger}, \hat{Q}] \times \hat{a}_q(t) - e^{-i\mathbf{k}_q \cdot \mathbf{r}_{\mu}} \hat{a}_q^{\dagger}(t) [\hat{Q}, \hat{\sigma}_{\mu} + \hat{\sigma}_{\mu}^{\dagger}] \}. \quad (\text{A.2})$$

The above involves \hat{a}_q which can be further solved from $d\hat{a}_q/dt = i[H, \hat{a}_q]$. The solution of \hat{a}_q reads

$$\hat{a}_q(t) = \hat{a}_q(0)e^{-i\omega_q t} + i \sum_{\mu} g_q e^{-i\mathbf{k}_q \cdot \mathbf{r}_{\mu}} \int_0^t dt' [\hat{\sigma}_{\mu}(t') + \hat{\sigma}_{\mu}^{\dagger}(t')] e^{-i\omega_q(t-t')}. \quad (\text{A.3})$$

With Born-Markov approximation, equivalently considering a relevant dynamical timescale of $\omega_e t \gg 1$ and $t \gg (r_{\mu\nu})_{\max}/c$ ($r_{\mu\nu} \equiv |\mathbf{r}_{\mu} - \mathbf{r}_{\nu}|$) [18], we derive the dynamical Heisenberg equations of $Q \equiv \langle \hat{Q} \rangle_0$ in Lindblad forms by assuming the vacuum initial bosonic fields $\langle \rangle_0$ (equivalent to the trace of the bosonic fields, leading to the reduced density matrix equations of the atoms),

$$\dot{Q}(t) = \sum_{\mu \neq \nu} i\Omega_{\mu,\nu} [\sigma_{\mu}^{\dagger} \sigma_{\nu}, Q] + \mathcal{L}(Q), \quad (\text{A.4})$$

$$\mathcal{L}(Q) = \sum_{\mu,\nu} \gamma_{\mu,\nu} \left[\sigma_{\mu}^{\dagger} Q \sigma_{\nu} - \frac{1}{2} (\sigma_{\mu}^{\dagger} \sigma_{\nu} Q + Q \sigma_{\mu}^{\dagger} \sigma_{\nu}) \right] \quad (\text{A.5})$$

The pairwise couplings $(\gamma_{\mu,\nu} + i2\Omega_{\mu,\nu})/2 \equiv J_{\mu,\nu}$ which can be defined as

$$J_{\mu,\nu} = \sum_q |g_q|^2 \int_0^{\infty} dt' e^{i\mathbf{k}_q \cdot (\mathbf{r}_{\mu} - \mathbf{r}_{\nu})} [e^{i(\omega_e - \omega_q)t'} + e^{-i(\omega_e + \omega_q)t'}], \\ = \sum_q |g_q|^2 \int_0^{\infty} dt' e^{i\mathbf{k}_q \cdot (\mathbf{r}_{\mu} - \mathbf{r}_{\nu})} [\pi\delta(\omega_q - \omega_e) + \pi\delta(\omega_q + \omega_e) + i\mathcal{P}(\omega_e - \omega_q)^{-1} - i\mathcal{P}(\omega_q + \omega_e)^{-1}]. \quad (\text{A.6})$$

For a 3D reservoir, we let $\sum_q \rightarrow \sum_{\vec{\epsilon}_q} \int_{-\infty}^{\infty} \frac{V}{(2\pi)^3} d^3q$ with two possible field polarizations $\vec{\epsilon}_q$. In spherical coordinates, we show the main results of $J_{\mu,\nu}$ in free space [18],

$$\gamma_{\mu,\nu}(\xi) \equiv \oint d\Omega_q [1 - (\hat{\mathbf{q}} \cdot \hat{\mathbf{p}})^2] \int_0^{\infty} dq q^2 \bar{g}_q^2 \frac{V}{(2\pi)^3} [\pi\delta(\omega_q - \omega_e) + \pi\delta(\omega_q + \omega_e)], \\ = \frac{3\Gamma}{2} \left\{ [1 - (\hat{\mathbf{p}} \cdot \hat{\mathbf{r}}_{\mu\nu})^2] \frac{\sin \xi}{\xi} + [1 - 3(\hat{\mathbf{p}} \cdot \hat{\mathbf{r}}_{\mu\nu})^2] \left(\frac{\cos \xi}{\xi^2} - \frac{\sin \xi}{\xi^3} \right) \right\}, \quad (\text{A.7})$$

$$\Omega_{\mu,\nu}(\xi) \equiv - \oint d\Omega_q [1 - (\hat{\mathbf{q}} \cdot \hat{\mathbf{p}})^2] \int_0^{\infty} dq q^2 \bar{g}_q^2 \frac{V}{(2\pi)^3} [i\mathcal{P}(\omega_q - \omega_e)^{-1} + i\mathcal{P}(\omega_q + \omega_e)^{-1}], \\ = \frac{3\Gamma}{4} \left\{ - [1 - (\hat{\mathbf{p}} \cdot \hat{\mathbf{r}}_{\mu\nu})^2] \frac{\cos \xi}{\xi} + [1 - 3(\hat{\mathbf{p}} \cdot \hat{\mathbf{r}}_{\mu\nu})^2] \left(\frac{\sin \xi}{\xi^2} + \frac{\cos \xi}{\xi^3} \right) \right\}, \quad (\text{A.8})$$

where $d\Omega_q$ denotes an integration of a solid angle of 4π , \mathcal{P} is the principal value of the integral, $\bar{g}_q^2 \equiv (d/\hbar)^2 [\hbar\omega_q/(2\epsilon_0 V)]$, $\hat{\mathbf{p}}$ aligns with the excitation field polarization, the intrinsic decay constant $\Gamma = d^2\omega_e^3/(3\pi\hbar\epsilon_0 c^3)$, and $\xi \equiv k_L|\mathbf{r}_\mu - \mathbf{r}_\nu|$ with $k_L = \omega_e/c$. $\gamma_{\mu,\nu}$ and $\Omega_{\mu,\nu}$ are respectively collective decay rates and frequency shifts in general for any two atoms in the ensemble. As $\xi \rightarrow 0$, Dicke's regime is reached where $\gamma_{\mu,\nu} \rightarrow \Gamma$, while $\Omega_{\mu,\nu}$ diverges. In the below, we review the results of $J_{\mu,\nu}$ in one- and two-dimensional reservoirs.

2. One-dimensional reservoir

From Eq. (A.6), the 1D reservoir gives [3] (note that V in \bar{g}_q is changed to L as a length scale of one-dimensional quantization volume)

$$J_{\mu,\nu} = \int_{-\infty}^{\infty} \frac{dq}{2\pi} \bar{g}_q^2 L e^{i\mathbf{k}_q \cdot (\mathbf{r}_\mu - \mathbf{r}_\nu)} [\pi\delta(\omega_q - \omega_e) + \pi\delta(\omega_q + \omega_e) + i\mathcal{P}(\omega_e - \omega_q)^{-1} - i\mathcal{P}(\omega_q + \omega_e)^{-1}]. \quad (\text{A.9})$$

We further obtain (let $x_{\mu,\nu} = x_\mu - x_\nu$ and dropping q in ω_q for brevity)

$$J_{\mu,\nu} = \int_0^\infty \frac{d\omega}{\pi} |\partial_\omega q(\omega)| \bar{g}_q^2 L \cos(\mathbf{k}_q x_{\mu,\nu}) [\pi\delta(\omega - \omega_e) + \pi\delta(\omega + \omega_e) + i\mathcal{P}(\omega_e - \omega)^{-1} - i\mathcal{P}(\omega + \omega_e)^{-1}]. \quad (\text{A.10})$$

Let $\Gamma_{1D} \equiv 2|\partial_\omega q(\omega)|_{\omega=\omega_e} \bar{g}_{k_L}^2 L$, where we keep the dispersion relation of the 1D coupling constant, and we obtain

$$J_{\mu,\nu} = \frac{\Gamma_{1D}}{2} \cos(k_L x_{\mu,\nu}) - \frac{i\mathcal{P}}{\pi} \int_{-\infty}^{\infty} d\omega \times \frac{\text{Re}[\partial_\omega q(\omega) \bar{g}_q^2 L e^{i\mathbf{k}_q \cdot (\mathbf{r}_\mu - \mathbf{r}_\nu)}]}{\omega - \omega_e}, \quad (\text{A.11})$$

which shows the Kramers-Kronig relation between real and imaginary parts of $J_{\mu,\nu}$. Finally the cooperative spontaneous emissions in 1D reservoir becomes [3]

$$J_{\mu,\nu} = \frac{\Gamma_{1D}}{2} [\cos(k_L x_{\mu,\nu}) + i \sin(k_L |x_{\mu,\nu}|)]. \quad (\text{A.12})$$

The above sinusoidal form shows the infinitely long-range dipole-dipole interaction between any atoms. This interaction, in contrast to 3D and later 2D results below, does not diverge in the part of collective frequency. Moreover, a true Dicke regime of $J_{\mu,\nu} = \Gamma_{1D}/2$ (no dipole-dipole interaction energy shift) when $\xi = 0$, 2π can be realized in 1D light-matter interacting system, making such system a potentially highly dynamical and strongly interacting platform. Meanwhile, when $\xi = \pi/2$, $3\pi/2$, RDDI in 1D reservoir allows only intrinsic decay and coherent exchange between atoms without dissipation.

3. Two-dimensional reservoir

Similarly from Eq. (A.6), the 2D reservoir has a quantization volume A , and we obtain $J_{\mu,\nu}$ in polar coordinates,

$$J_{\mu,\nu} = \int_0^\infty \frac{q \bar{g}_q^2 A}{(2\pi)^2} dq \int_0^{2\pi} d\theta [1 - (\hat{\mathbf{q}} \cdot \hat{\mathbf{p}})^2] e^{i\mathbf{k}_q \cdot \mathbf{r}_{\mu,\nu}} [\pi\delta(\omega - \omega_e) + \pi\delta(\omega + \omega_e) + i\mathcal{P}(\omega_e - \omega)^{-1} - i\mathcal{P}(\omega + \omega_e)^{-1}]. \quad (\text{A.13})$$

Consider the real part of $J_{\mu,\nu}$ first and $\hat{\mathbf{q}}$ has polar angle θ to the \hat{z} . We assume that $\mathbf{r}_{\mu,\nu}$ is along \hat{z} and $\hat{\mathbf{p}}_{\parallel}$ aligns with a polar angle θ' to \hat{z} where $\hat{\mathbf{p}}_{\parallel} = \hat{\mathbf{p}} \sin \phi$ and $\hat{\mathbf{p}}_{\perp} = \hat{\mathbf{p}} \cos \phi$ with an angle ϕ to \hat{y} . We then obtain

$$\begin{aligned} \text{Re}[J_{\mu,\nu}] &= \int_0^\infty \frac{q \bar{g}_q^2 A}{(2\pi)^2} dq \int_0^{2\pi} d\theta [1 - (\cos \theta \cos \theta' + \sin \theta \sin \theta')^2 \sin^2 \phi] e^{i\xi \cos \theta} \pi\delta(\omega - \omega_e), \\ &= \frac{\Gamma_{2D}}{2} \frac{1}{\pi} \int_0^{2\pi} d\theta [1 - (\cos \theta \cos \theta' + \sin \theta \sin \theta')^2 \sin^2 \phi] e^{i\xi \cos \theta} \end{aligned} \quad (\text{A.14})$$

where $\Gamma_{2D} \equiv 2k_L |\partial_\omega q(\omega)|_{\omega=\omega_e} \bar{g}_{k_L}^2 A \pi^2 / (2\pi)^2$.

To further calculate $\text{Re}[J_{\mu,\nu}]$, we need the following integrals,

$$\int_0^{2\pi} e^{ia \cos \theta} d\theta = 2\pi J_0(|a|), \quad (\text{A.15})$$

$$\int_0^{2\pi} \cos^2 \theta e^{ia \cos \theta} d\theta = 2\pi \left(\frac{J_1(a)}{a} - J_2(a) \right), \quad (\text{A.16})$$

$$\int_0^{2\pi} \sin^2 \theta e^{ia \cos \theta} d\theta = 2\pi \frac{J_1(|a|)}{|a|}, \quad (\text{A.17})$$

$$\int_0^{2\pi} \sin \theta \cos \theta e^{ia \cos \theta} d\theta = 0, \quad (\text{A.18})$$

where $J_n(a)$ represents the Bessel functions of the first kind. Then we obtain

$$\begin{aligned} \text{Re}[J_{\mu,\nu}] &= \frac{\Gamma_{2D}}{2} 2 \left[J_0(\xi) - \frac{J_1(\xi)}{\xi} + (\hat{\mathbf{p}} \cdot \hat{\mathbf{r}}_{\mu,\nu})^2 J_2(\xi) \right], \\ &\equiv \frac{\Gamma_{2D}}{2} f(\xi). \end{aligned} \quad (\text{A.19})$$

The $\text{Re}[J_{\mu,\nu}]$ and $\text{Im}[J_{\mu,\nu}]$ should satisfy the Kramers-Kronig

relation, and we obtain

$$J_{\mu,\nu} = \frac{\Gamma_{2D}}{2} f(\xi) - \frac{i\mathcal{P}}{2\pi} \int_0^\infty d\omega \left(\frac{1}{\omega - \omega_e} + \frac{1}{\omega + \omega_e} \right) \times (k_L |\partial_\omega q(\omega)| \bar{g}_q^2 A/2) f(\omega |\mathbf{r}_\mu - \mathbf{r}_\nu|/c),$$

$$= \frac{\Gamma_{2D}}{2} [f(\xi) + ig(\xi)], \quad (\text{A.20})$$

where

$$f(\xi) \equiv 2 \left[J_0(\xi) - \frac{J_1(\xi)}{\xi} + (\hat{\mathbf{p}} \cdot \hat{\mathbf{r}}_{\mu,\nu})^2 J_2(\xi) \right], \quad (\text{A.21})$$

$$g(\xi) \equiv 2Y_0(\xi) - 2\frac{Y_1(\xi)}{\xi} + 2(\hat{\mathbf{p}} \cdot \hat{\mathbf{r}}_{\mu,\nu})^2 Y_2(\xi) - \frac{4}{\pi\xi^2} [1 - 2(\hat{\mathbf{p}} \cdot \hat{\mathbf{r}}_{\mu,\nu})^2], \quad (\text{A.22})$$

and $Y_n(\xi)$ represents the Bessel functions of the second kind. The above $g(\xi)$ can be derived by using the following inte-

grals,

$$\mathcal{P} \int_0^\infty da \frac{J_0(a)}{a \mp b} = -\frac{\pi}{2} [Y_0(b) \pm H_0(b)], \quad (\text{A.23})$$

$$\mathcal{P} \int_0^\infty da \frac{J_1(a)}{a(a \mp b)} = -\frac{2 + \pi b [Y_1(b) \pm H_1(b)]}{2b^2}, \quad (\text{A.24})$$

$$\mathcal{P} \int_0^\infty da \left(\frac{J_2(a)}{a-b} + \frac{J_2(a)}{a+b} \right) = -\frac{4}{b^2} - \pi Y_2(b), \quad (\text{A.25})$$

where $H_n(b)$ is the Struve function.

All the results for the RDDI in 1D, 2D, and 3D reservoirs are reciprocal. This means that $J_{\mu,\nu} = J_{\nu,\mu}$, preserving the time reversal symmetry for light scattering between the μ th and ν th atoms. Similar 2D RDDI has been studied in point scatterers using 2D coupled dipole equations [47], and super- and subradiance properties are investigated in details with the above 2D RDDI [48].

-
- [1] P. Lodahl, S. Mahmoodian, S. Stobbe, A. Rauschenbeutel, P. Schneeweiss, J. Volz, H. Pichler, and P. Zoller, *Nature* **541**, 473 (2017).
 - [2] D. E. Chang, J. S. Douglas, A. González-Tudela, C.-L. Hung, H. J. Kimble, *Rev. Mod. Phys.* **90**, 031002 (2018).
 - [3] A. González-Tudela and D. Porras, *Phys. Rev. Lett.* **110**, 080502 (2013).
 - [4] K. Y. Bliokh, A. Y. Bekshaev, and F. Nori, *Nat. Commun.* **5**, 3300 (2014).
 - [5] K. Y. Bliokh and F. Nori, *Phys. Rep.* **592**, 1 (2015).
 - [6] R. Mitsch, C. Sayrin, B. Albrecht, P. Schneeweiss, and A. Rauschenbeutel, *Nat. Commun.* **5**, 5713 (2014).
 - [7] I. Shomroni, S. Rosenblum, Y. Lovsky, O. Bechler, G. Guendelman, and B. Dayan, *Science* **345**, 903 (2014).
 - [8] I. J. Luxmoore, *et. al.*, *Phys. Rev. Lett.* **110**, 037402 (2013).
 - [9] I. Söllner, *et. al.*, *Nat. Nanotechnol.* **10**, 775 (2015).
 - [10] A. R. Hamann, C. Müller, M. Jerger, M. Zanner, J. Combes, M. Pletyukhov, M. Weides, T. M. Stace, and A. Fedorov, *Phys. Rev. Lett.* **121**, 123601 (2018).
 - [11] A. Grankin, P. O. Guimond, D. V. Vasilyev, B. Vermersch, and P. Zoller, *Phys. Rev. A* **98**, 043825 (2018).
 - [12] H. H. Jen, *J. Phys. B: At. Mol. Opt. Phys.* **52**, 065502 (2019).
 - [13] K. Stannigel, P. Rabl, and P. Zoller, *New J. Phys.* **14**, 063014 (2012).
 - [14] T. Ramos, H. Pichler, A. J. Daley, and P. Zoller, *Phys. Rev. Lett.* **113**, 237203 (2014).
 - [15] H. Pichler, T. Ramos, A. J. Daley, and P. Zoller, *Phys. Rev. A* **91**, 042116 (2015).
 - [16] J. Kumlin, S. Hofferberth, and H. P. Büchler, *Phys. Rev. Lett.* **121**, 013601 (2018).
 - [17] R. H. Dicke, *Phys. Rev.* **93**, 99 (1954).
 - [18] R. H. Lehmberg, *Phys. Rev. A* **2**, 883 (1970).
 - [19] M. Gross and S. Haroche, *Phys. Rep.* **93** 301 (1982).
 - [20] H. H. Jen, *Phys. Rev. A* **85**, 013835 (2012).
 - [21] H. H. Jen, *Ann. of Phys. (N.Y.)* **360**, 556 (2015).
 - [22] M. O. Araújo, I. Krešić, R. Kaiser, and W. Guerin, *Phys. Rev. Lett.* **117**, 073002 (2016).
 - [23] S. J. Roof, K. J. Kemp, M. D. Havey, and I. M. Sokolov, *Phys. Rev. Lett.* **117**, 073003 (2016).
 - [24] S. Jennewein, *et al.*, *Phys. Rev. Lett.* **116**, 233601 (2016).
 - [25] Bromley, S. L. *et al.*, *Nat. Commun.* **7** 11039 (2016).
 - [26] B. Zhu, J. Cooper, J. Ye, and A. M. Rey, *Phys. Rev. A* **94**, 023612 (2016).
 - [27] E. Shahmoon, D. S. Wild, M. D. Lukin, and S. F. Yelin, *Phys. Rev. Lett.* **118**, 113601 (2017).
 - [28] M. O. Scully, *Phys. Rev. Lett.* **115**, 243602 (2015).
 - [29] W. Guerin, M. O. Araújo, and R. Kaiser, *Phys. Rev. Lett.* **116**, 083601 (2016).
 - [30] G. Facchinetti, S. D. Jenkins, and J. Ruostekoski, *Phys. Rev. Lett.* **117**, 243601 (2016).
 - [31] H. H. Jen, M.-S. Chang, and Y.-C. Chen, *Phys. Rev. A* **94**, 013803 (2016).
 - [32] R. T. Sutherland and F. Robicheaux, *Phys. Rev. A* **94**, 013847 (2016).
 - [33] R. J. Bettles, S. A. Gardiner, and C. S. Adams, *Phys. Rev. A* **94**, 043844 (2016).
 - [34] H. H. Jen, *Phys. Rev. A* **96**, 023814 (2017).
 - [35] S. D. Jenkins, J. Ruostekoski, N. Papisimakis, S. Savo, and N. I. Zheludev, *Phys. Rev. Lett.* **119**, 053901 (2017).
 - [36] A. Asenjo-Garcia, M. Moreno-Cardoner, A. Albrecht, H. J. Kimble, D. E. Chang, *Phys. Rev. X* **7**, 031024 (2017).
 - [37] H. H. Jen, M.-S. Chang, and Y.-C. Chen, *Sci. Rep.* **8**, 9570 (2018).
 - [38] H. H. Jen, *Sci. Rep.* **8**, 7163 (2018).
 - [39] F. Le Kien, S. Dutta Gupta, K. P. Nayak, and K. Hakuta, *Phys. Rev. A* **72**, 063815 (2005).
 - [40] F. L. Kien and K. Hakuta, *Phys. Rev. A* **77**, 013801 (2008).
 - [41] F. Le Kien and A. Rauschenbeutel, *Phys. Rev. A* **95**, 023838 (2017).
 - [42] P. Solano, P. Barberis-Blostein, F. K. Fatemi, L. A. Orozco, and S. L. Rolston, *Nat. Commun.* **8**, 1857 (2017).
 - [43] C. W. Gardiner, *Phys. Rev. Lett.* **70** 2269 (1993).
 - [44] H. J. Carmichael, *Phys. Rev. Lett.* **70** 2273 (1993).
 - [45] C. Sayrin, C. Clausen, B. Albrecht, P. Schneeweiss, and A. Rauschenbeutel, *Optica* **2**, 353 (2015).
 - [46] C. L. Hung, A. González-Tudela, J. I. Cirac, and H. J. Kimble, *Proc. Natl Acad. Sci.* **113**, E4946 (2016).
 - [47] C. E. Máximo, N. Piovella, Ph. W. Courteille, R. Kaiser, and R.

Bachelard, Phys. Rev. A **92**, 062702 (2015).

[48] H. H. Jen, Sci. Rep. **9**, 5804 (2019).